Production Well Targeting at Newberry Volcano EGS Demonstration

Trenton T. Cladouhos, Matthew E. Uddenberg, Michael W. Swyer, Susan Petty, and Yini Nordin

AltaRock Energy, Inc. 4010 Stone Way North, Suite 400, Seattle WA 98103

tcladouhos@altarockenergy.com

ABSTRACT

The Newberry Volcano EGS Demonstration is a five year field project designed to demonstrate recent technological advances for engineered geothermal systems (EGS) development. Advances in reservoir stimulation, diverter, and monitoring are being tested in a hot (>300 ºC), dry well (NWG 55-29) drilled in 2008. In the fall of 2014, 9,500 m^3 (2.5 million gallons) of groundwater were injected at a maximum wellhead pressure of 195 bar (2850 psi) over 4 weeks of hydraulic stimulation. Injectivity changes, thermal profiles and seismicity indicate that fracture permeability in well NWG 55-29 was enhanced. The fifteen-station microseismic array (MSA) located 398 seismic events, ranging in magnitude from M 0 to M 2.26. The next step is to drill a production well into the EGS reservoir. Advanced analysis of the microseismic data including hand picking of first arrivals, moment tensors derivations, relative relocations, and velocity model improvements have resulted in new higher-quality microseismic catalogs. These catalogs have been combined by relative weighting and gridding of seismic densities, resulting in probability-based maps and cross-sections, which have been used to plan a production well trajectory. The microseismic locations and times were also used to develop a reservoir diffusivity model, which can be used to evaluate stimulation plans such as dual-well stimulation.

1. INTRODUCTION

Newberry Volcano is a shield volcano located in central Oregon, about 35 km south of the city of Bend and 65 km east of the crest of the Cascade Range. The Newberry EGS Demonstration is being conducted on federal geothermal leases and National Forest Service lands located in the Deschutes National Forest, adjacent to Newberry National Volcanic Monument.

The goals of the demonstration include (Osborn et al., 2010):

- Create an EGS reservoir,
- Stimulate multiple zones in existing well NWG 55-29 using thermally-degradable zonal isolation materials (TZIM) and associated technologies,
- Confirm EGS reservoir viability through a flow-back test of the injected water,
- Drill one or two production wells to intersect the EGS reservoir, and
- Demonstrate EGS viability through a circulation test.

During Phase 1 of the demonstration an environmental assessment (BLM, 2011), project-specific Induced Seismicity Mitigation Plan (ISMP)(AltaRock, 2011), and technical plans (Osborn et al., 2010; Cladouhos et al., 2011; 2012) were completed. This allowed the project to proceed to the Phase 2.1, well stimulation. In Phase 2.1, a microseismic array (MSA) was installed, stimulation pumps procured and installed, and the well stimulated for 7 weeks (Cladouhos et al., 2013a, 2013b; Petty et al., 2013). During the first stimulation, the well head pressure (WHP) reached 167 bar (2,450 psi), 40,000 m^3 (11 million gallons) of water were injected, and over 170 microearthquakes were located, illuminating an EGS reservoir at an average depth of 1000 m (3,200 ft). Further study and well surveys in 2013 determined that well repairs and a second stimulation would be necessary to create a deeper, hotter EGS reservoir. Phase 2.2 of the demonstration was performed from late August to November 2014. A more complete report of the 2014 stimulation can be found in Cladouhos et al. (2015) and AltaRock (2015). This paper is focused on efforts to plan the production well, 55A-29.

2. 2014 STIMULATION SUMMARY

On Sept. 23, rig up and testing of the stimulation system was completed and a low pressure step-rate test from 83 to 138 bar (1,200 to 2,000 psi) WHP was conducted overnight on Sept. 23 to 24 (Figure 1). At these pressures, flow rates were below 2.3 L/s (30 gpm) indicating a very low injectivity index. After surface piping leaks were repaired on Sept. 24, the step rate test continued to 180 bar (2,600 psi) WHP. The flow rates at this pressure exceeded 4.5 L/s (60 gpm) with a noticeable increase in injectivity to 0.025 L/s bar (0.03 gpm/psi) during the steps from 166 to 180 bar) 2,400 to 2,600 psi (Figure 1). Injectivity continued to increase until Oct. 1 to 0.05 L/s bar (0.06 gpm/psi). This injectivity improvement was permanent as indicated by low pressure step-rate testing on Nov. 11 and high pressure step-rate testing on Oct. 15.

Flow rate spikes (e.g. on Sept. 27 on Figure 1) occurred when step rate pressure changes caused temporary high flows followed by a decline in flow rate over an hour to lower flows. Thermohydrologic (TH) modeling using TOUGH2 (Sonnenthal et al., 2015) indicates that this behavior can be explained by compression of the water due to the pressure increase in the well bore and formation.

Numerical modelling presented in Cladouhos et al. (2011) predicted that microseismicity and injectivity improvement would initiate at a WHP of 93 bar (1,350 psi) and that 134 to 152 bar (1,950–2,200 psi) would be sufficient to reach the required reservoir volume goal. The 2012 stimulation (Cladouhos et al., 2013a, 2013b) seemed to confirm this prediction with injectivity improvements and deep seismicity (>8,000 ft, >2.4 km) initiating at a WHP of 93 bar (1,360 psi) and four additional deep seismic events occurring at a WHP of 132 bar

Cladouhos et al.

(1,910 psi). Thus the need to exceed 172 bar (2,400 psi) WHP to promote stimulation in 2014 was unexpected. The practical effect is that the stimulation pumps reached their maximum pressure of 197 bar (2,850 psi) on Sept. 29, the sixth day of the stimulation. Surface equipment, shoe depth and regulatory agreements also specified that the stimulation pressures be kept below 207 bar (3,000 psi), so the pump performance was not the only limit preventing significantly higher pressures.
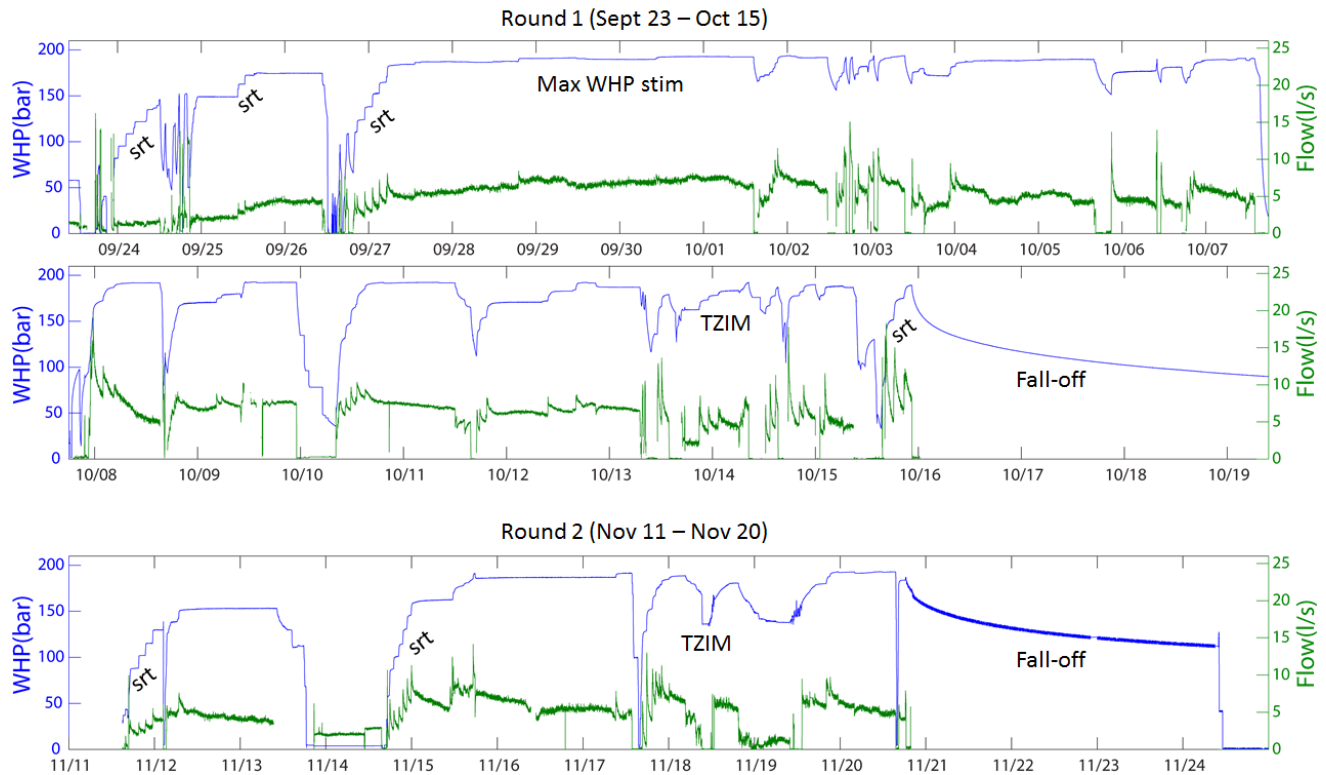

Figure 1: Well head pressure (blue) and flow rate (green) records during round 1 (top two panels) and round 2 (bottom panel) of 2014 stimulation. Periods of step rate tests are indicated by "srt".

3. MICROSEISMICITY

Microseismic monitoring is a key component of EGS development, as it is the best way to map the progress and extent of EGS growth. The primary focus of this paper is analysis of the micro-seismicity and how it was used to plan the production well, 55A-29.

3.1 Microseismic array and Background events

A microseismic array was installed in August 2012 as part of Phase 2.1. Two-Hz 3 component geophones were installed at seven surface sites and eight borehole sites (Figure 2). The 15 stations stream continuous data via cell phone modem to a server running acquisition software at AltaRock's office in Seattle where the continuous data are saved and archived. Triggered waveforms were sent to Lawrence Berkeley National Lab (LBNL) for locating and publishing to their public website (LBNL, 2015). Microseismic events were also analyzed by the Pacific Northwest Seismic Network (PNSN, 2015) and Foulger Consulting, who focused on deriving moment tensor solutions, calculating relative locations, and improving the crustal model (Julian and Foulger, 2004).

The regional seismic network at Newberry Volcano has improved greatly in the past two years. In 2009, the only station was NCO, a single-component, short-period seismometer on the east flank and only four microearthquakes (M 1.3-2.2) were detected in Newberry in the prior 25 years (PNSN, 2015). In 2011, the USGS installed six three-component broadband seismometers and one three-component short-period sensor (PNSN, 2015). Four of the borehole stations in the AltaRock Newberry MSA (NN32, NN19, NN17, and NN21) as well as the strong motion sensor (NNVM) were also added to the PNSN network. The seismic coverage of Newberry Volcano is now comprehensive, with events smaller than M 0.0 being locatable. During the 2012 stimulation, over 170 events were located in the stimulation zone with magnitudes between M 0.0 and M 2.3 (Cladouhos et al., 2013a). Between 3/1/2013 and 9/20/2014 there were about 60 natural seismic events located in the Newberry edifice (PNSN, 2015). The increase in the number of earthquakes outside of the EGS stimulation zone (>1 km from 55-29) located at Newberry Volcano since 2012 does not indicate increased seismicity due to natural causes or EGS activities. Instead, it is a consequence of the much improved seismic network.
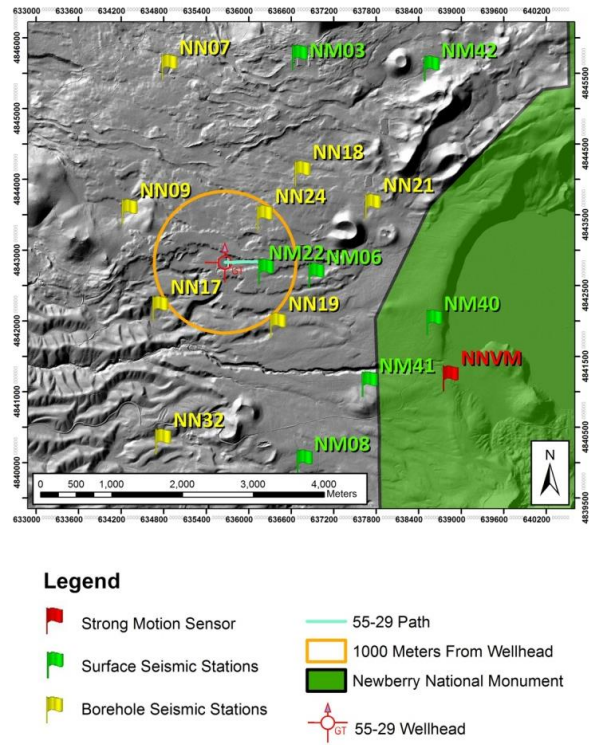
Figure 2: MSA station locations, EGS well 55-29, and Newberry National Volcanic Monument (green shading).

3.2 Microseismicity rate during stimulation

As is typical of hydraulic well stimulation, the rate of seismicity correlates to well head pressure and flow rate (Figure 3). Microseismicity did not commence until a WHP of 180 bar (2,600 psi) was exceeded. Over 30 events per day were located on Oct. 1-3 after the WHP exceeded 193 bar (2,800 psi). After five days of increasing seismicity and improving injectivity, the seismicity rate dropped by more than 50% by Oct. 6. Additional modeling (i.e. Sonnenthal et al, 2015) and further analysis have been undertaken to better understand the drop in seismicity rate and early peaking of the injectivity improvement.
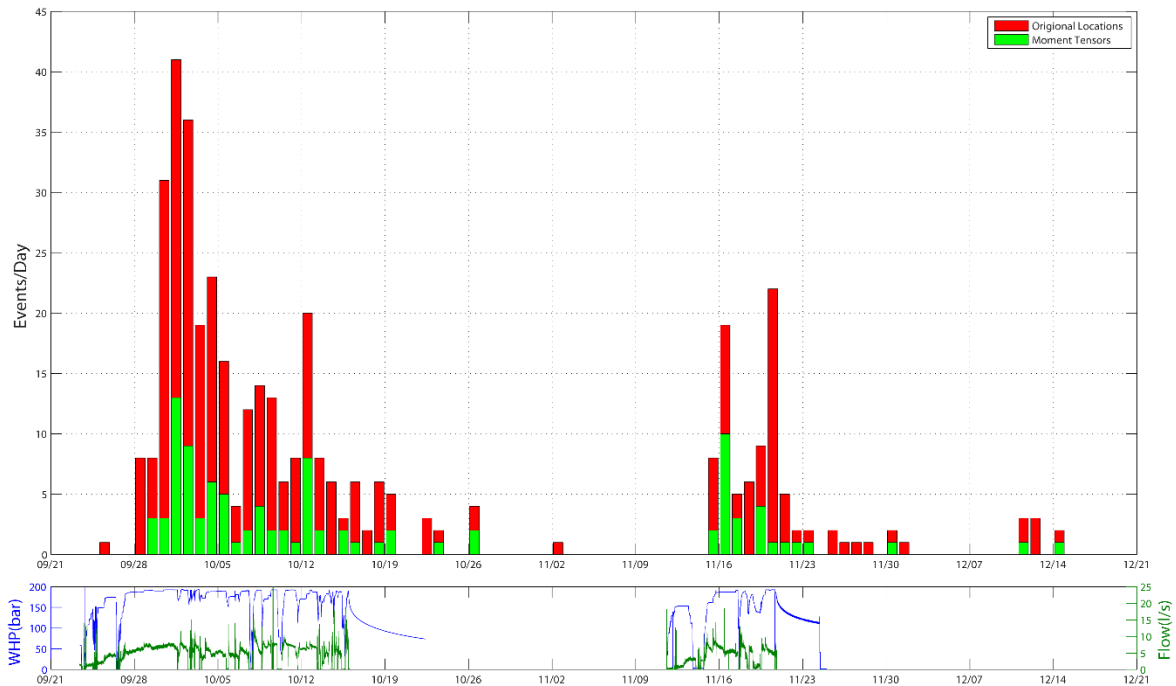

Figure 3: Temporal histogram of microseismic events. Green bars show the 99 events for which moment tensors were derived using the methods described in Julian and Folger (2004). Red bars show all 398 events located in the stimulation zone.

3.3 EGS Seismic Event Locations

Triggered waveforms were analyzed by multiple means. First, the seismic acquisition software automatically identified events, generating preliminary P- and S-wave picks and locations. The software sent an alert email to project scientists and seismologists including a map of the preliminary location. In addition, waveforms were sent to LBNL and Foulger Consulting. The P&S-wave arrival time measurements for all triggered events were reviewed by a seismologist within a day, resulting in a location catalog of 398 hand-picked events that was used to assess EGS growth during the stimulation operations. The initial locations of the 398 microseismic events are diffuse and plot up to 500 m from the injection well (Figure 4).
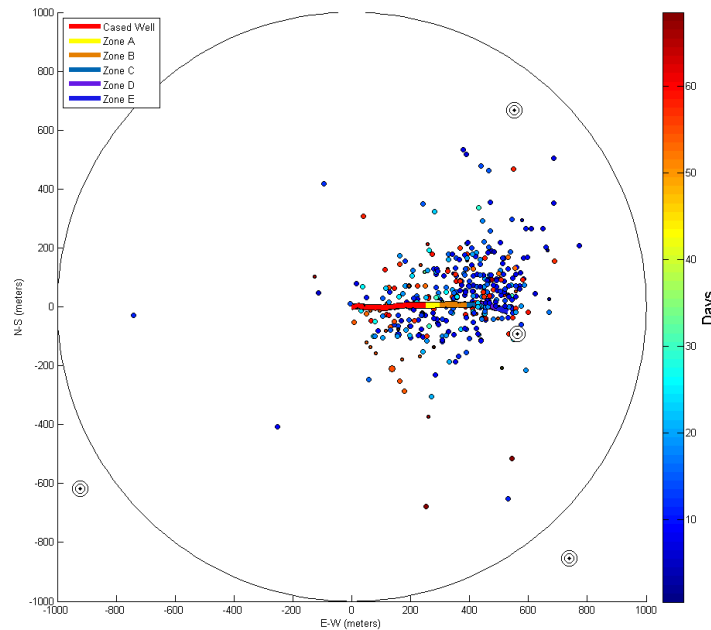

Figure 4: Initial locations of microseismic events in relation to well bore. The surface location of the well is at the center of the circle which is 1 km in radius. The well path is to the east, thee colors indicated casing (red) and geologic zones shown by the key at the top left. The timing (days after start) of the microseismic events is indicated by the color scale on the right.

3.4 Relative Relocations

Lawrence Berkeley National Lab (LBNL) was one of three groups responsible for collecting and analyzing micro-seismic data. Initial locations were analyzed using automated arrival time software which showed the results on the LBNL Induced Seismicity website (LBNL, 2015). These initial results were scattered and were determined to have significant location error.

After the stimulation, all the events were reviewed and arrival times for each event were handpicked by seismologists at LBNL. In addition the ratio of P-wave velocity to S-wave velocity (Vp/Vs) was refined. This parameter effects the seismic event depths and can be poorly constrained. This uncertainty was reconciled by calculating locations and depths using different Vp/Vs ratios and then determining which depth ranges best explained the data gathered in the wellbore. Zones of outflow from the well are some of the best constrained data gathered during the stimulation. Multiple PTS surveys indicated that one of the major flowing zones in the well was near the bottom of the well. The Vp/Vs ratio which put the deepest seismicity near the outflow zone at the bottom of the well is 1.7. This ratio is also consistent the shallowest seismicity locating just below the casing shoe and the highest seismic density locating at the other known major outflow zone at approximately 2,520 meters (8,265 ft) TVD. This hand-picked catalog of locations (red dots in Figure 5) is one of the four catalogs considered in siting the production well.

Locations were then relatively relocated using a software package called tomoDD (Zhang and Thurber, 2003). This program, a double difference tomography model, uses absolute and differential arrival time data to determine event locations and velocity structures. Using tomoDD and refining the parameters of the velocity model, LBNL arrived at what they determined to be their best set of data (blue dots in Figure 5). Comparison of the original hand-picked locations and the relocated dataset, shows a systemic shift of the seismic events. The average event was relocated at an azimuth of 213° at a radius of 189 meters away and 72 meters deeper than the original auto-picked events Figure 6.

3.5 Moment Tensors

Microseismicity in geothermal reservoirs can involve several different physical processes (Julian et al., 1998; Miller et al., 1998), including simple shear slip on planar faults, tensile cracking, and rapid fluid motion. Understanding these processes is critical to understanding hydroshearing mechanics in EGS projects. Traditional "fault-plane solutions" assume only simple shear slip occurs, which ignores both processes associated with opening and closing cracks and fluid flow. For this reason, a moment-tensor approach should be used in EGS
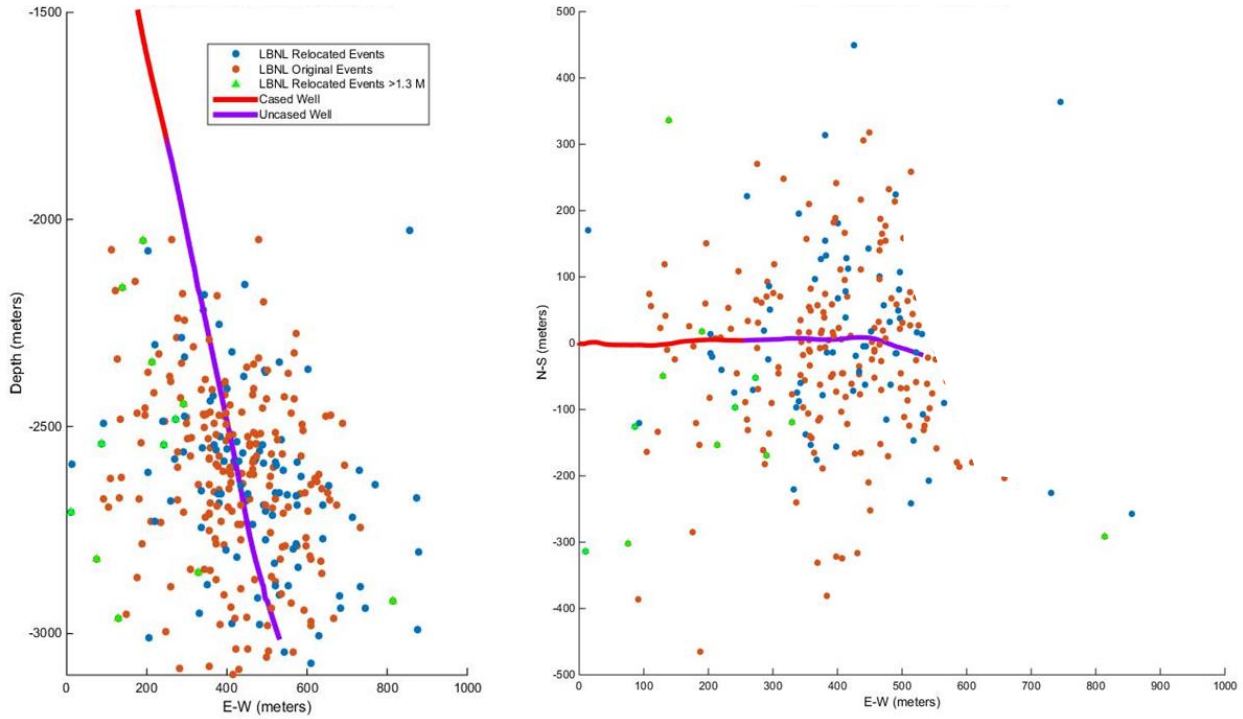
Figure 5: North-looking cross section (left) and map view (right) showing original LBNL locations (red), relative relocations (blue), and largest (M>1.3) relocated events (green).
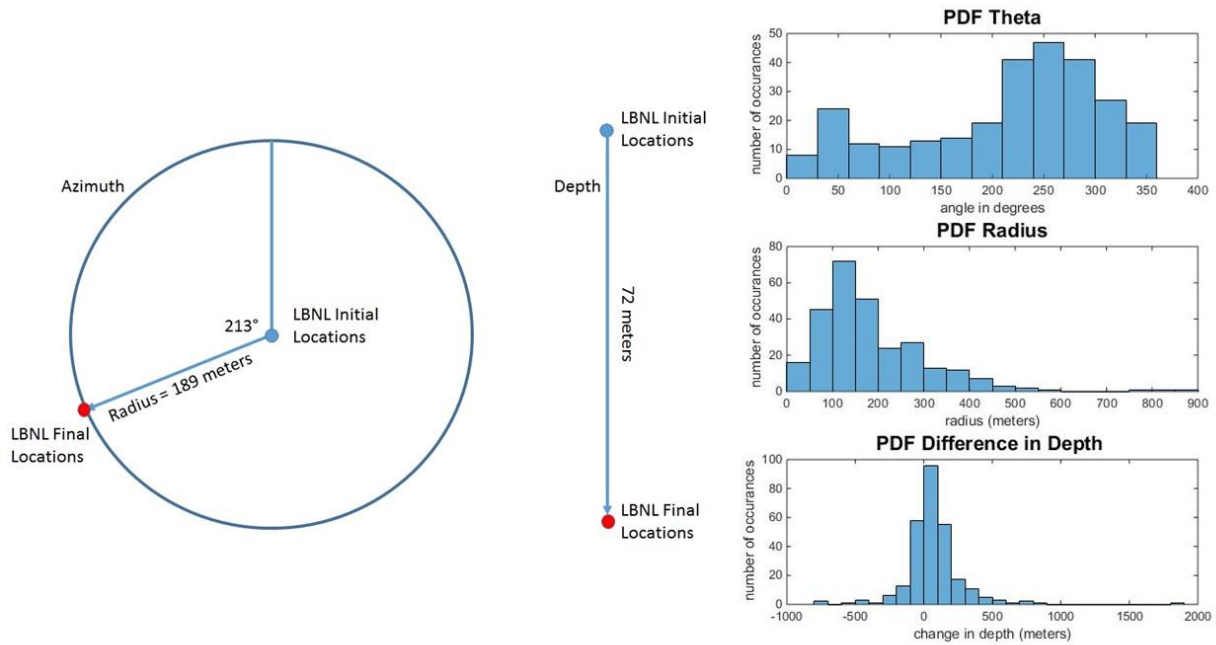

Figure 6. Statistics of event relocations. Left: average change in direction for all relocations. Right: histograms for the direction of change, horizontal distance change, and depth change.

stimulations, which requires more information than just P-wave polarities. The most effective and readily obtained information is P- and S-phase amplitudes (Julian and Foulger, 1996, 2004).

Moment tensors are displayed graphically using source-type diagrams (Hudson et al., 1989). This has been applied to many natural and industrially induced micro-earthquake sequences, including geothermal and hydrocarbon reservoirs and EGS stimulations (Julian and

Foulger, 1996; Julian et al., 2010; Miller et al., 1998). A source-type diagram (Figure 7) illustrates the deviation from a pure earthquake double-couple (DC) source at the center in terms of a volumetric component, explosion on top and left or implosion on bottom and right. Tectonic earthquakes typically fall near the center point of the plot (labeled DC). Injection-induced seismicity, which involves an underground change in volume, may require non-DC source-types.

Moment tensor solutions were calculated for 99 events. The source-type plot (Figure 7) indicates a wide variety of source mechanisms ranging from double couple to opening cracks (+Crack) to closing cracks (-Crack). This variety may be due to a relatively low differential stress and stimulation of variable volcanic features (e.g., dikes, flow boundaries, ring fractures). The corresponding P and T axes (Figure 8) are approximate indicators of the principal stresses. The T-axis average which approximates the minimum principal stress direction, has a N12°E trend and plunges 57° to the north. The P-axes, which approximate the maximum principal stress direction, are sub-horizontal with a 270° range in trends (Figure 8).

The spatial distribution of the P and T axes is plotted in Figure 9 along with volume loss/gain by plotting the k-values for the source types, which represent the isotropic component of the moment tensor and are also the vertical axis on the source type plot (Figure 7). Positive values indicate a relative volume gain, and negative values indicate a relative volume loss. The vertical distribution of the source types further reveals where similar source types are grouped at depth, which may indicate individual structural features. The small grouping of positive k source types just to the southeast of the bottom of the well exhibits a northwest striking sub-vertical planar feature which has a strong right-lateral component.
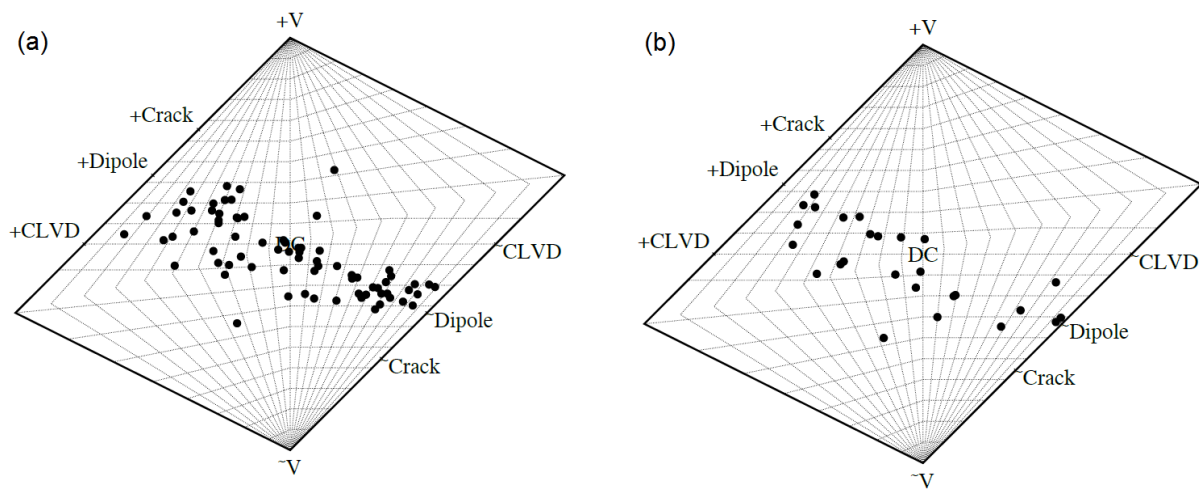

Figure 7: Source-type plots of 100 moment tensors. (a) 74 events for round 1 and (b) 26 events for round 2.
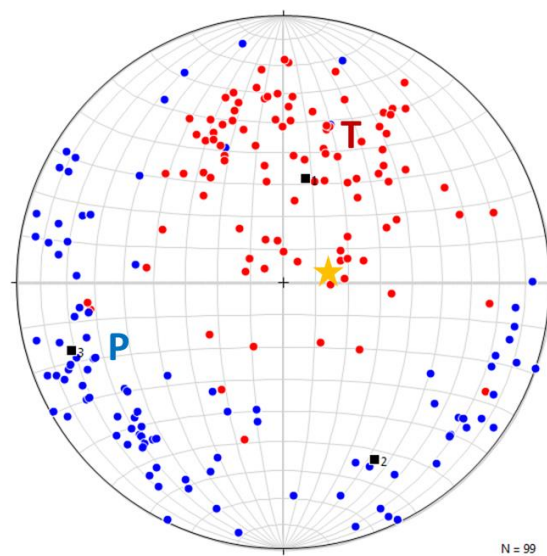

Figure 8: Lower hemisphere stereonet P (blue) and T (red) axes of moment tensors determined by Foulger Consulting. Black square is the average T-axis (N12°E, 57°). Gold star shows the azimuth and plunge (N86°E, 74°) of the proposed production interval of 55A-29.
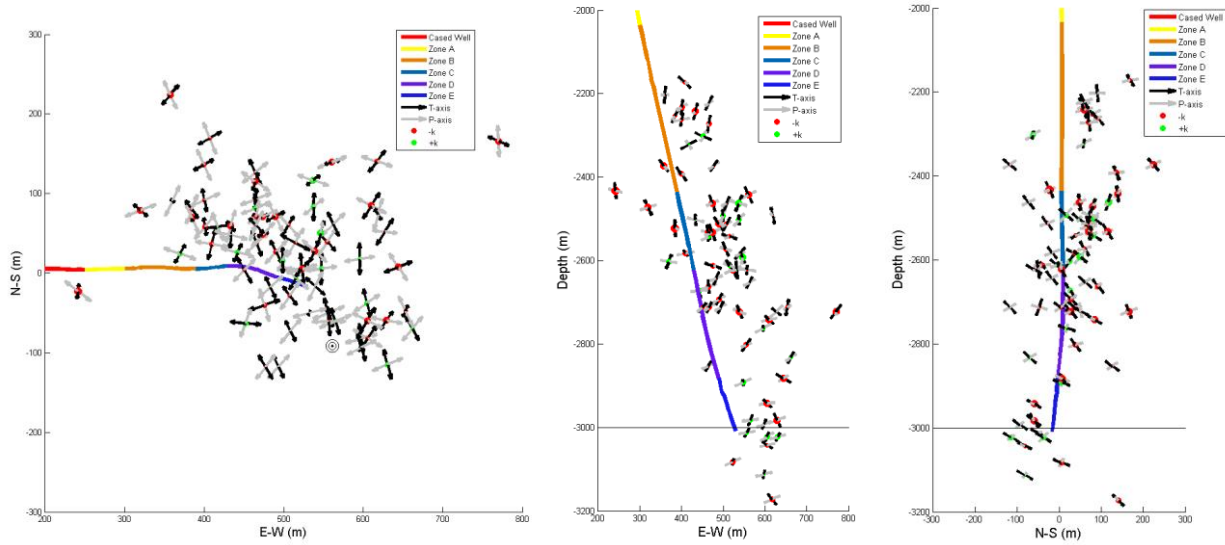
Figure 9: Spatial distribution of P and T axis around well with volume gain (green, k+) and volume loss (red, k-). Map view (left), north-looking cross section (center) and west-looking cross section (right).

3.6 Seismic Density Plots

To reconcile the differences in seismic event locations between different teams of seismologists AltaRock decided to summarize the seismic catalogs from a different perspective. Rather than debate the relative accuracy of each methodology in an attempt to arrive at the "best" single catalog, we instead calculate the probability that an event has occurred within a defined grid cell volume. There is a range of error associated with each seismic catalog due to assumptions made about the velocity model and the software used to help locate events. To enhance signal and reduce noise, we combine the four catalogs to create seismic density plots. This is done by assigning relative weights to the individual datasets based on perceived location quality (Table 1). For example, the dataset "Foulger MT Locations" has the highest weight (40%) because the events in this catalog were carefully hand-picked on seismograms rotated to ray path coordinates (up, radial, transverse). The dataset labeled "Original Locations" is the least constrained, so these events are given the lowest weight (10%). A side-effect of this weighting scheme is that the largest (M>0.7), and presumably best located, 99 events (Table 1) are represented in all four catalogs, thus will be counted four times with a total weight of one. Meanwhile, the smallest 38 events (M<0.0) will only be counted once, with a total weight of just 10%. A weighting ratio between the small events and the bigger events is similar to weighting by seismic moment.

Table 1. Table showing relative weights for each dataset shown in the seismic density plots.

Catalog	Number of Events	Weight
Original Locations	400	10%
LBNL Hand-picked Locations	362	20%
LBNL Relative Relocations	278	30%
Foulger MT Locations	99	40%

The stimulated volume was gridded using 50x50 m cells on the horizontal plane and 100 m cells along the vertical axis. The grid cells are asymmetrical with respect to depth because the vertical location error is generally twice the horizontal location error (Ernest Majer, pers. comm., 2015). The size of the horizontal grid cells roughly correlates with the horizontal error associated with the best located events (LBNL relocs), which have a precision of 44 m (144 ft). In testing, a finer grid resulted in discontinuities in the density and a coarser grid did not capture the structure of the seismic cloud. After assigning a weight to each dataset (Table 1) all points contained within a single grid cell, or bin, are summed to create a specific value for that cell. This creates a 3D histogram, which outlines the rock volumes most likely to have had multiple seismic events occur during stimulation (Figure 10).

The zones with highest seismic density are located near the well at 2,500-2,600 m (8,200– 8,528 ft). This is associated with a known outflow zone at 2,560 m MD (8,400 ft). The seismicity from this exit point seems to extend 150 m to 200 m (490-660 ft) away from the well. The combined catalog seismic cloud is elongated and denser in the East-West direction. Generally, events tend to get deeper as one goes from West to East (Figure 10). In the North-South direction the seismic cloud is less coherent than in the East-West direction and events become deeper as one goes from North to South. While the trend of events getting deeper in the North-South direction are likely

Cladouhos et al.

the result of structural elements down hole, the trend of events getter deeper in the West-East direction is the result of the angle of the well. Another interesting result from these seismic plots are that there is clearly a continuous seismically stimulated area, where events are located close to each other and clumped around the well, and a discontinuous seismically active stimulated area, where there are isolated patches of seismicity which appear to be unrelated to the denser seismic cloud near the wellbore. These isolated patches of seismicity are likely caused by one of two reasons. Either there are elongated permeable elements, such as fractures, where the seismicity is occurring along the terminus of these elements, or pressure increases in the reservoir are causing failure of fractures in the far field without being infiltrated by water.

3.6 Production Well Path

Based on the seismic density maps, a production well path was designed to intersect the outer edge of the stimulated zone indicated by micro-seismicity (green path in Figure 10). The casing would be run to 2,200 m, the elbow shown in this schematic. This well path can be described as *below and south of 55-29*. An alternative path to intersect the micro-seismicity could be designed *above and north of 55-29*; however, this would require more difficult and risky directional drilling.

Because most of the best-located seismic events do not extend beyond 250 m from the stimulated well, the spacing between the well pair is 200-250 m (Figure 11). This is closer than is generally considered to be the optimal spacing for EGS well doublets (350-500 m). While this might lead to a shorter economic lifetime for the initial Newberry EGS well doublet, AltaRock considers that the conservative approach is to insure that the wells connect, so that a circulation test and further dual-well stimulation can be performed.
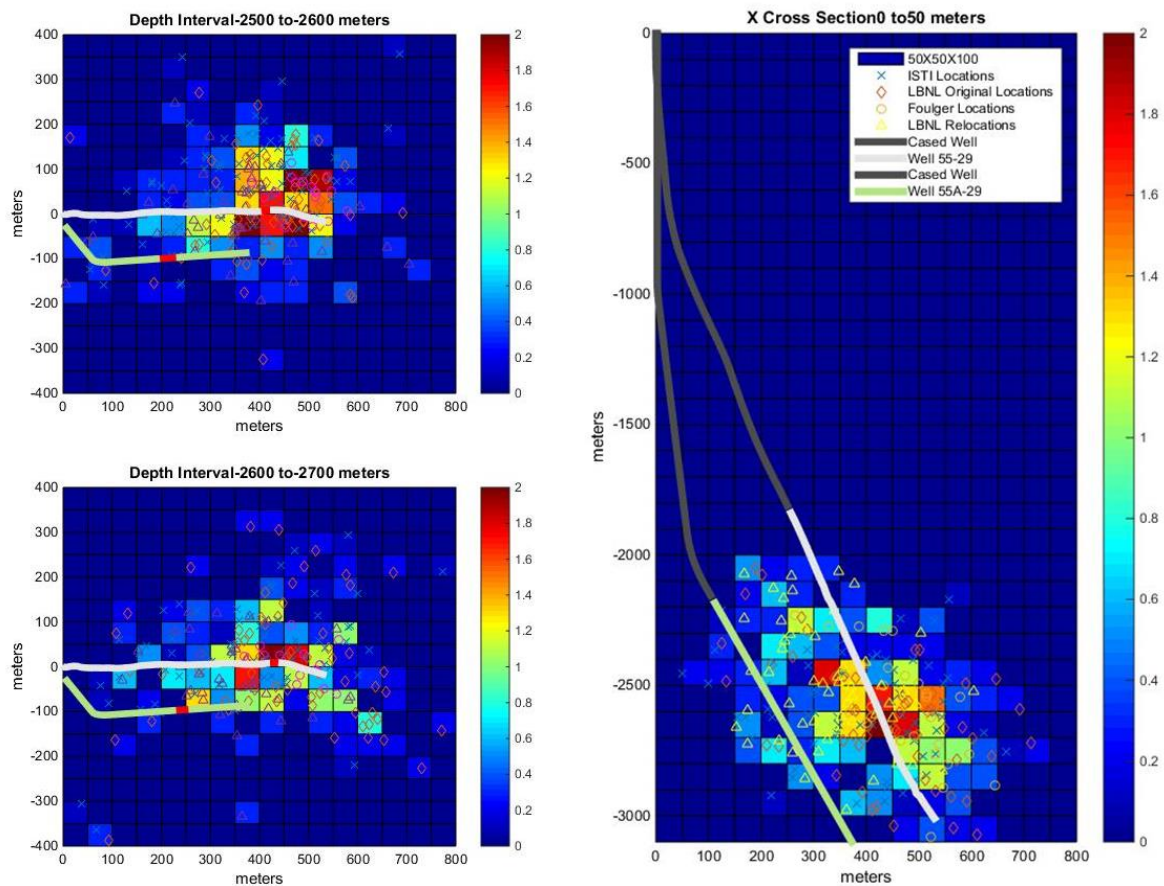

Figure 10: Seismic density plots for well 55-29. Map at depth slices of 2,400-2,500 m (top left) 2,700-2,800 m (bottom left). Red sections of the proposed well path are well intersections with the depth slices. Cross section at 0-50 m south of the well (right). White path is stimulated well (55-29) and green path is planned producer (55A-29).

The close spacing between the wells is partly mitigated by the high temperatures at Newberry. At a measured depth of 2,200 m, where the wells are 250 m apart the static temperature is 250 ºC and at 3,000 m the static temperature is 330 ºC. The reduction in spacing with depth is by design, a shorter pathway at higher rock temperature will not be cooled as fast, and will ensure greater probability of a connection across the highest temperature zone. The proposed well path allows for another potential mitigation step. If thermal breakthrough occurs, the initial production interval could be plugged and the well re-drilled with a greater well spacing – further below and south of the original hole.
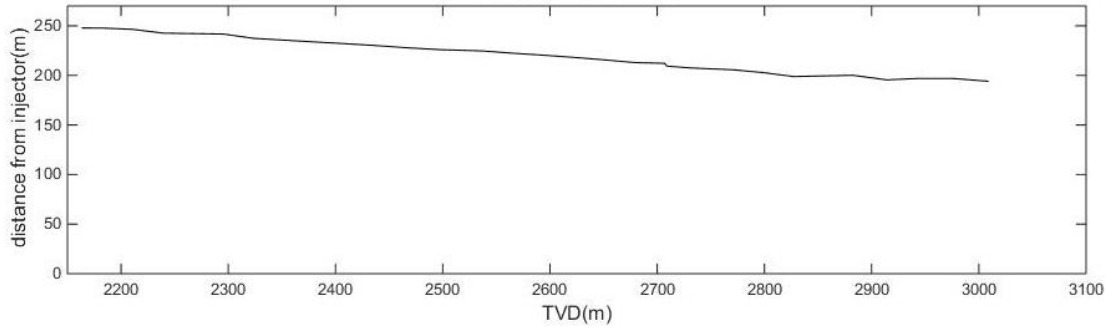
Figure 11. Well spacing vs. depth between the injection (55-29) and production wells (55A-29).

AltaRock (2015) develops preliminary thermal modeling to determine the potential power production and temperature decline with the average 225 m well spacing required by the seismic analysis above. Using a multiple parallel fracture model (Gringarten, 1975) with six planar fractures, a flow rate of 25 kg/s, and an initial geofluid production temperature of 275 °C, the production temperature would remain above 200 °C for 3.5 years (or 14 years at 12.5 kg/s). In this scenario, the initial gross power production from the doublet would be 3.9 MW. An economic EGS power plant could not be sustained with this rate of temperature decline. However, the significant knowledge gained by producing from the first doublet at Newberry, would likely lead to design of future re-drills, stimulations, and new wells that would be economic.

3.7 Reservoir Diffusivity

To hydraulically characterize the seismically active stimulated region around the well, an underlying mechanism of pore-pressure diffusion is applied to the temporal distribution of events around the point of injection. This is done by assuming a point source of pressure from the bottom of the well and measuring the distance of each event from the point source for the length of the stimulation. The spatial distribution of the events over time has a triggering front with a parabolic signature (Parotidis, et al., 2004):

$$r = \sqrt{4\pi D t} \qquad \text{Eq. 1}$$

Where r is the distance of the triggering front, t is time, and D is the hydraulic diffusivity of the surrounding rock. After pumping of the well has ceased, and the well is shut-in, seismicity continues to spread from the point source of pressure but develops a parabolic back front from the point source:

$$r = \sqrt{6Dt\left(\frac{t}{t_0} - 1\right) ln\left(\frac{t}{t-t_0}\right)} \qquad \text{Eq. 2}$$

Where t_0 is the shut-in time. The LBNL relocated event distances with time were fit to parabolic triggering and back fronts for both round 1 and 2 stimulations using a hydraulic diffusivity value of 0.006 m^2/s with the wellhead pressure and flow (Figure 12). Assuming a porosity (ϕ) of 0.03, dynamic viscosity (μ) of 8.5×10^{-5} Pa-s for 150°C water, and total system compressibility (c_t) of 9.4×10^{-10} Pa^{-1}, this equates to a permeability (k) of 1.44×10^{-17} m^2 using:

$$k = D\phi\mu c_t \qquad \text{Eq. 3}$$

The hydraulic diffusivity value can also be used to predict pore-pressure diffusion from the injection well during a stimulation using:

$$P_p(r,t) = \frac{q}{4\pi D r} erfc\left(\frac{r}{\sqrt{4Dt}}\right) \qquad \text{Eq. 4}$$

Where P_p is the pore pressure as a function of radius and time, q is the point-source pressure, or down-hole pressure in the well and $erfc$ is the complementary error function. Using an average WHP of 193 bar (2,800 psi) or a downhole pressure of 425 bar (6,163 psi) during the stimulation, the pore-pressure distribution for round 1 is shown in Figure 13a, showing the pore-pressure approaching zero 250m away from the well which is the extent of the seismic cloud from the well. Figure 13b is a pore-pressure diffusion model with a second well 200m away. Both wells in this scenario are stimulated with a WHP of 241 bar (3,500 psi) or 473 bar (6,860 psi) downhole pressure for the same amount of time as round 1 (22.5 days). Although the pore-pressure near the well is unchanged, the pore-pressure directly in between the wells is twice as high as a result of a dual stimulation. Thus pressurizing both wells can promote connectivity between the two wells.
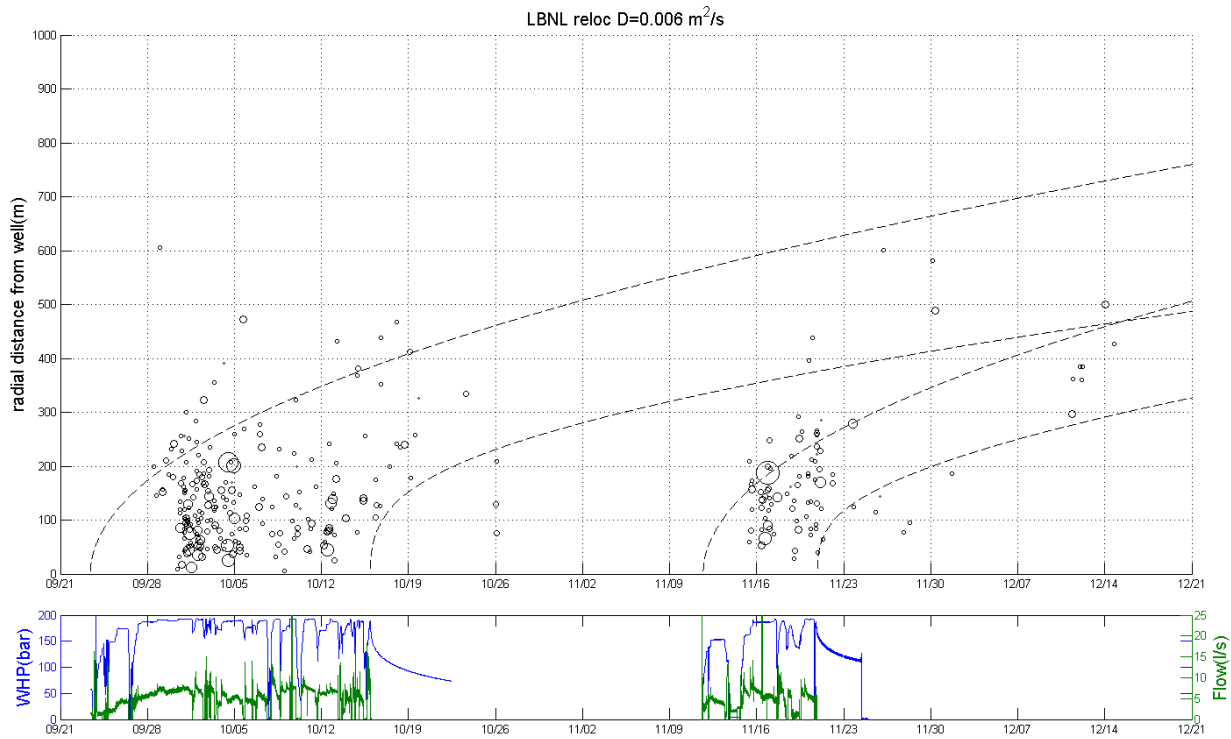
Figure 12: Radius vs time for events (sized by magnitude) for both rounds of stimulation with wellhead pressure and injection rate.
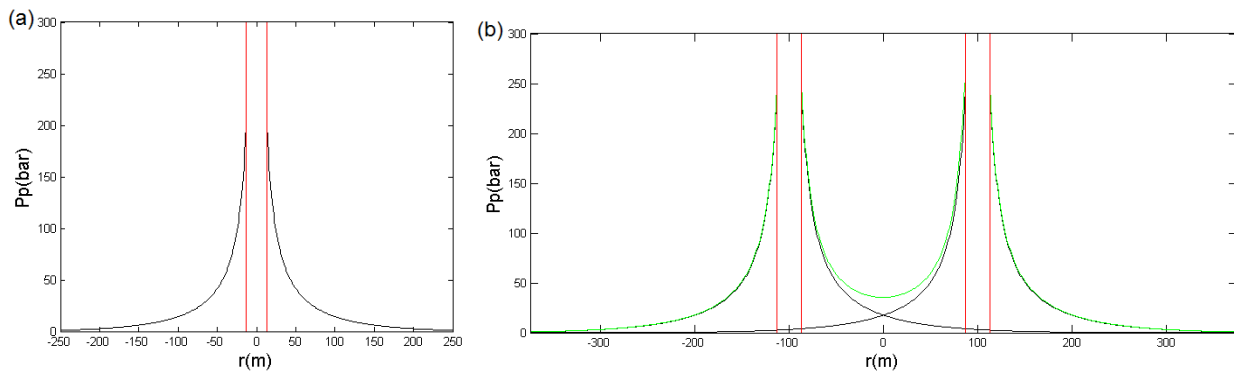

Figure 13: Pore-pressure away from exit point at 2,895 m (9,498 ft) MD in black for (a) single well and (b) well doublet, showing the sum of both wells in green.

4. CONCLUSIONS

About 2.5 million gallons (9,500m^3) of ground water was injected during a total of 4 weeks of hydraulic stimulation of NWG 55-29 in the fall of 2014. Well head pressures greater than 2450psi (165bar) were required to improve injectivity of the well, which was significantly higher than expected. A permanent injectivity improvement from 0.01 gpm/psi to 0.04 gpm/psi was achieved. However, much of the stimulation was run near the limits of the pumps, well head, surface piping and permits, limiting the ability further improve injectivity.

Locations for 398 microseismic events were determined using the MSA installed in 2012. Advanced analysis of the microseismic data including hand picking of first arrivals, moment tensors, relative relocations, and velocity model improvements have resulted new higher-quality microseismic catalogs. These catalogs have been combined by relative weighting and gridding of seismic densities, resulting in probability-based maps and cross-sections, which have been used to plan a production well trajectory. The microseismic locations and times were also used to develop a reservoir diffusivity model, which can be used to evaluate stimulation plans such as dual-well stimulation.

In order to insure connectivity to 55-29, plans will also be made to stimulate the production well, 55A-29, both individually and in concert with the 55-29. A stimulation plan and equipment that allows for higher WHP to be used on the production well will also be developed Drilling and stimulation of the production well is planned for the 2015 field season.

Acknowledgments

Disclaimer

This paper was prepared as an account of work sponsored by an agency of the United States Government. Neither the United States Government nor any agency thereof, nor any of their employees, makes any warranty, express or implied, or assumes any legal liability or responsibility for the accuracy, completeness, or usefulness of any information, apparatus, product, or process disclosed, or represents that its use would not infringe privately owned rights. Reference herein to any specific commercial product, process, or service by trade name, trademark, manufacturer, or otherwise does not necessarily constitute or imply its endorsement, recommendation, or favoring by the United States Government or any agency thereof. The views and opinions of authors expressed herein do not necessarily state or reflect those of the United States Government or any agency thereof.

REFERENCES

AltaRock, Newberry EGS Demonstration Induced Seismicity Mitigation Plan, 64 pp. plus 14 appendices. Available at: http://altarockenergy.com (2011)

AltaRock, Newberry EGS Demonstration Phase 2.2 Report, 132 pp. plus 8 appendices. Internal report to the DOE (2015).

BLM, Newberry Volcano Enhanced Geothermal System (EGS) Demonstration Project, Environmental Assessment, 148 pp. plus 2 appendices, Available at http://www.blm.gov/or/districts/prineville/plans/newberryegs/index.php. (2011).

Cladouhos, T.T., Petty, S., Swyer, M.W., Uddenberg, M.E, and Nordin, Y. Results from Newberry Volcano EGS Demonstration, *Proceedings*, 40th Workshop on Geothermal Reservoir Engineering Stanford University, Stanford, CA (2015).

Cladouhos, T.T., Petty, S., Nordin, Y., Moore, M., Grasso, K., Uddenberg, M., Swyer, M., Julian, B., and Foulger, G. Microseismic Monitoring of Newberry Volcano EGS Demonstration, *Proceedings*, 38th Workshop on Geothermal Reservoir Engineering Stanford University, Stanford, CA, (2013).

Cladouhos, T.T., Petty, S., Nordin, Y., Moore, M., Grasso, K., Uddenberg, M. and Swyer, M.W. Stimulation Results from the Newberry Volcano EGS Demonstration, *GRC Transactions*, **37**, 133-140, (2013).

Cladouhos, T.T., Osborn, W.L., and Petty, S., Newberry Volcano EGS Demonstration—Phase I Results, *Proceedings*, 37th Workshop on Geothermal Reservoir Engineering Stanford University, Stanford, CA (2012).

Cladouhos, T.T., M. Clyne, M. Nichols, S. Petty, W.L. Osborn, and L. Nofziger. Newberry Volcano EGS Demonstration Stimulation Modeling, *GRC Transactions*, **35**, 317-322, (2011).

Gringarten A.C., Witherspoon P. A., Yuzo Ohnishi. Theory of heat extracted from fractured hot dry rock. Journal of Geophysical Research. DOI:10.1029/JB080i008p01120, (1975).

Hudson, J.A., Pearce, R.G., Rogers, R.M. Source type plot for inversion of the moment tensor. Journal of Geophysical Research: Solid Earth, 94, 765–774., (1989).

Julian, B.R., Foulger, G.R. Earthquake mechanisms from linear-programming inversion of seismic-wave amplitude ratios. Bulletin of the Seismological Society of America, 86, 972–980 (1996).

Julian, B.R., Miller, A.D., Foulger, G.R. Non-double-couple earthquakes 1. Theory. Reviews of Geophysics, 36, 525–549, (1998).

Julian, B.R. and G.R. Foulger, Microearthquake focal mechanisms – A tool for monitoring geothermal systems, *Geotherm. Res. Council Bull.*, **33**, 166-171, (2004).

Julian, B.R., Foulger, G.R., Monastero, F.C., Bjornstad, S. Imaging hydraulic fractures in a geothermal reservoir. Geophysical Research Letters, 37, L07305, (2010).

LBNL, http://esd.lbl.gov/research/projects/induced_seismicity/egs/newberry.html (2015).

Miller, A.D., Foulger, G. R., Julian, B.R.Non-double-couple earthquakes 2. Observations. Reviews of Geophysics, 36, 551–568, (1998).

Osborn, W.L., Petty, S., Cladouhos, T.T., Iovenitti, J., Nofziger, L., Callahan, O., Perry, D.S. and Stern P.L. Newberry Volcano EGS Demonstration – Phase I Results, *GRC Transactions*, **35**, 499-505, (2011).

Petty, S. Nordin, Y., Glassely, W. and Cladouhos, T. Improving Geothermal Project Economics with Multi-zone Stimulation: Results from the Newberry Volcano EGS Demonstration, *Proceedings*, 38th Workshop on Geothermal Reservoir Engineering Stanford University, Stanford, CA, (2013).

PNSN, http://pnsn.org/volcanoes/newberry (2015).

Shapiro, S. A., C. Dinske, C. Lagenbruch, and F. Wenzel. Seismogenic index and magnitude probability of earthquakes induced during reservoir fluid stimulations, *The Leading Edge*, 304-309, (March 2010).

Cladouhos et al.

Shapiro, S. A., and C. Dinske. Scaling of seismicity induced by nonlinear fluid-rock interaction, *J.Geophys. Res.,* **114,** B09307, doi:10.1029/2008JB006145 (2009).

Sonnenthal, E.L., Smith, J.T., Cladouhos, T., Kim, J., and Yang, L. Thermal-Hydrological-Mechanical-Chemical Modeling of the 2014 EGS Stimulation Experiment at Newberry Volcano, Oregon. PROCEEDINGS, Fortieth Workshop on Geothermal Reservoir Engineering Stanford University, Stanford, CA (2015).

Zhang, H. and Thurber, C. H. Double-Difference Tomography: The Method and Its Application to the Hayward Fault, California. *Bulletin of the Seismological Society of America*, **93**, No. 5, pp. 175-1889, (2003).